Astronomy & Astrophysics manuscript no. deb˙keck˙aa˙final
September 29, 2010

Orbital and physical parameters of eclipsing binaries from the ASAS catalogue

II. Two spotted $M < 1$ M$_\odot$ systems at different evolutionary stages.

K. G. Hełminiak[1] and M. Konacki[1,2]

[1] Nicolaus Copernicus Astronomical Center, Department of Astrophysics, ul. Rabiańska 8, 87-100 Toruń, Poland
e-mail: xysiek@ncac.torun.pl, maciej@ncac.torun.pl
[2] Astronomical Observatory, Adam Mickiewicz University, ul. Słoneczna 36, 60-286 Poznań, Poland

Received ...; accepted ...

ABSTRACT

Aims. We present the results of our detailed spectroscopic and photometric analysis of two previously unknown < 1 M$_\odot$ detached eclipsing binaries: ASAS J045304-0700.4 and ASAS J082552-1622.8.
Methods. With the *HIgh Resolution Echelle Spectrometer* (HIRES) on the Keck-I telescope, we obtained spectra of both objects covering large fractions of orbits of the systems. We also obtained *V* and *I* band photometry with the 1.0-m Elizabeth telescope of the South African Astronomical Observatory (SAAO). The orbital and physical parameters of the systems were derived with the PHOEBE and JKTEBOP codes. We investigated the evolutionary status of both binaries with several sets of widely-used isochrones.
Results. Our modelling indicates that (1) ASAS J045304-0700.4 is an old, metal-poor, active system with component masses of $M_1 = 0.8452 \pm 0.0056$ M$_\odot$, $M_2 = 0.8390 \pm 0.0056$ M$_\odot$ and radii of $R_1 = 0.848 \pm 0.005$ R$_\odot$ and $R_2 = 0.833 \pm 0.005$ R$_\odot$, which places it at the end of the Main Sequence evolution – a stage rarely observed for this type of stars. (2) ASAS J082552-1622.8 is a metal-rich, active binary with component masses of $M_1 = 0.703 \pm 0.003$ M$_\odot$, $M_2 = 0.687 \pm 0.003$ M$_\odot$ and radii of $R_1 = 0.694^{+0.007}_{-0.011}$ R$_\odot$ and $R_2 = 0.699^{+0.011}_{-0.014}$ R$_\odot$. Both systems show significant out-of-eclipse variations, probably owing to large, cold spots. we also investigated the influence of a third light in the second system.

Key words. binaries: eclipsing – binaries: spectroscopic – stars: fundamental parameters – stars: late type – stars: individual: ASAS J045304-0700.4, ASAS J082552-1622.8

1. Introduction

Eclipsing binaries provide the absolute values for a number of physical parameters of stars that are crucial for testing the stellar structure and for evolution models. These parameters are especially needed for stars with masses below 1 M$_\odot$. They are the most numerous in the Galaxy, yet our models often fail to accurately reproduce their properties (Ribas et al. 2008). In order to perform reliable tests of the models, we need to derive masses, radii, and other parameters with a precision of 3% or better (Blake et al. 2008; Clausen et al. 2008). In recent years progress in the detection and characterization of the K and M-type eclipsing binaries was made (Shkolnik et al. 2008; Çakırlı& İbanoğlu 2010; Irwin et al. 2009). But not every binary from the limited sample of low-mass systems satisfies the 3% accuracy criterion, which makes every new datapoint important.

In this paper we present for the first time the orbital and physical parameters of two new detached eclipsing spectroscopic binaries (DEBs), both of which have the component masses below 1 $M_\odot$ – ASAS J045304-0700.4 (hereafter ASAS-04) and ASAS J082552-1622.8 (hereafter ASAS-08). We reach 0.5 % level of precision for the masses and radii. Both objects seem to be interesting from the evolutionary point of view. ASAS-04 is most likely an active, old, metal-poor and spotted object that seems to be near the end of its main-sequence stage. ASAS-08 on the contrary is younger, metal rich, more active and covered with larger spotted areas. we present our observations and their analysis below.

2. ASAS-04 and ASAS-08

2.1. ASAS-04 (GSC 04749-00560)

The eclipsing binary ASAS J045304-0700.4 is the fainter of the two objects – its apparent *V* magnitude depending on the catalogue is between 11.125 (Kharchenko 2001) and 11.35 mag (Pojmański 2002). Our photometry (Sect. 3.2) indicates $V = 11.240 \pm 0.005$ and $I = 10.374 \pm 0.005$ mag at the maximum. Its eclipsing nature was noted for the first time in the *ASAS Catalog of Variable Stars*[1] (ACVS; Pojmański 2002). The system is classified in ACVS as an eclipsing detached binary (ED) with an amplitude of the photometric variation of 0.29 mag. The ASAS photometric dataset now spans more than nine years and provides a complete phase coverage. A quick look at the ASAS light curve allows one to conclude that the given period $P = 1.6224\,d$ can be improved. When phased with the correct period (see Table 2), the ASAS curve shows no clear out-of-eclipse variations. ASAS-04 is likely associated with the faint ROSAT X-ray source 1RXS J045304.1-070011 ($F_x = 1.073 \times 10^{-12}$ erg cm^{-2} s^{-1}). The total ROSAT positional error of 12" for this source is a

[1] http://www.astrouw.edu.pl/asas/

bit smaller than the separation between ROSAT and the ASAS-04 position in the visual ($\sim$ 13", even including a small but measurable proper motion).

2.2. ASAS-08 (GSC 05998-01918, EUVE J0825-16.3)

This system's magnitude in V available from various sources is between 10.20 (Pojmański 2002) and 10.42 mag (Urban et al. 2001). Our photometry – $V = 10.142 \pm 0.003$ and $I = 8.708 \pm 0.003$ mag at the maximum – seems to favour the first value. The binary was identified as a faint extreme ultraviolet (Lampton et al. 1997) and a soft X-ray source (1RXS J082551.4-162244, $F_x = 3.556 \times 10^{-12}$ erg cm^{-2} s^{-1}; Voges et al. 1999). It was later optically identified as a dKe or dMe star (Polomski et al. 1997). ASAS-08 was reported as a double-lined spectroscopic binary (SB2) by Christian & Mathioudakis (2002), who also provided the equivalent widths of the H_α and H_β lines separately for every component. The first spectroscopic orbital solution was recently derived by Montes et al. (2007). They obtained five high-resolution echelle spectra, two of which were at the orbital phase $\phi = 0$. They also reported a presence of a third component with a velocity consistent with the systemic velocity of the binary. The eclipsing pair itself was previously identified by the *Hipparcos* satellite (HIP 41322, NLTT 1915, PPM 715320) to be a part of the visual double system CCDM 08259-1623. The brightness ratio from the Montes et al. (2007) data is consistent with the magnitude difference of 2.37 mag reported in the *Hipparcos* catalogue. Note also that the new reduction of *Hipparcos* data (van Leeuwen 2007) gives the parallax of 21.83 $\pm$ 2.25 mas or the distance of 45.8 $\pm$ 4.7 pc.

Eclipses in this system were firstly noted in the ACVS (Pojmański 2002). For ASAS-08 the dataset spans more than nine and covers the full orbit. The ACVS orbital period $P = 1.52852\,d$ is also not perfect. The ASAS light curve shows no clear evidence of the out-of-eclipse variations. However, our data (see Sect. 4.3) clearly show a presence of spots, which are expected in active late-type stars. These spots and the third light have made our photometric analysis quite challenging.

3. Observations

3.1. Spectroscopy

Both ASAS-04 and ASAS-08 are targets from our sample of candidate late-type ASAS detached eclipsing binaries (DEBs). In order to derive accurate radial velocities (RVs) that would allow us to precisely estimate the masses, we obtained a series of high-resolution ($R \sim 60000$) echelle spectra with the *HIgh Resolution Echelle Spectrometer* (HIRES) on the 10-m Keck-I telescope. The spectra were taken during four observing runs between September 2004 and October 2005 – nine observations with the exposure times of 900 s for ASAS-04 and eight with the exposure time of 600 s for ASAS-08. The resulting signal-to-noise ratio for a collapsed pixel (SNR) was $\sim$110 and 170 at $\lambda \simeq 6000$ Å for ASAS-04 and ASAS-08 respectively. The spectra were taken with the iodine cell and reduced as described by Konacki (2005). The application of the disentangling technique (Konacki et al. 2009) did not improve the RVs.

Radial velocities for both systems were obtained with our implementation of the two-dimensional cross-correlation technique (TODCOR Zucker & Mazeh 1994). As templates we used synthetic spectra computed with the ATLAS code (Castelli & Kurucz 2003). The velocities for every epoch are collected in Table 1. The formal errors, usually between 100 and 200 m s^{-1}, were computed from the scatter between the used echelle orders and are underestimated. To obtain a reduced χ^2 equal to $\sim$1, we added in quadrature a constant additional error, which for ASAS-04 was 0.61 km s^{-1} for the primary and 0.44 km s^{-1} for the secondary and for ASAS-08 — 0.6 and 0.5 km s^{-1} for the primary and secondary respectively. These values are nearly equal to the resulting *rms*' of the orbital fit. Even though the iodine cell is used, the resulting RV precision is hampered by the rotational broadening of spectral lines in both systems ($v \sin i \sim 25$ km s^{-1}) and the activity of the components, which is most likely the origin of the additional RV error. Because of the broadening we could not perform any reliable abundance analysis. Many weaker lines could not be recognized and the measured equivalent widths or depths were too inaccurate[2].

Table 1. Barycentric radial velocities of ASAS-04 and ASAS-08

Date (TDB) -2450000.0	v_1 km s^{-1}	±	*O-C*	v_2 km s^{-1}	±	*O-C*
ASAS-04						
3277.0930	148.40	0.62	0.16	-40.38	0.58	-0.23
3277.1274	153.98	0.58	-0.15	-45.75	0.49	0.32
3329.0271	152.32	0.58	-0.06	-45.08	0.49	-0.78
3330.0147	-48.11	0.58	-0.29	157.53	0.49	0.24
3454.7577	-44.19	0.60	0.46	153.45	0.55	-0.63
3456.7734	12.64	0.77	1.44	97.76	0.80	-0.04
3655.1046	154.07	0.58	-0.08	-45.57	0.48	0.51
3656.1196	-43.04	0.59	-0.74	152.00	0.50	0.29
3657.0408	124.30	0.58	-0.09	-16.05	0.48	0.11
ASAS-08						
3329.1417	-50.01	0.70	-0.34	121.32	0.60	0.12
3330.1258	131.99	0.70	-0.46	-65.06	0.60	0.00
3454.7773	-47.84	0.70	-0.68	118.61	0.60	-0.06
3455.8200	14.36	0.71	0.42	56.63	0.62	0.51
3456.7692	118.61	0.70	0.51	-51.23	0.61	-0.79
3655.1169	-13.07	0.70	0.53	84.05	0.60	-0.24
3656.1383	-18.66	0.70	1.02	89.58	0.60	-0.89
3657.1184	135.97	0.70	0.03	-68.36	0.60	0.25

3.2. Photometry

The original ASAS light curves of ASAS-04/08 are not sufficiently accurate enough for a precise determination of the orbital and physical parameters. Therefore we carried out a three-week observing run on the 1.0-m Elizabeth telescope at the South African Astronomical Observatory (SAAO) in January 2008. We used a 1024×1024 STE4 camera with the Johnson V and Cousins I filters. The field of view was 317×317 arcseconds (0.31 arcsec/pix). In order to keep the SNR at a relatively high level, exposure times varied depending on the observing conditions. The data were processed with the standard data reduction tasks available in the *IRAF* package[3].

For the photometric calibration we selected up to five of the brightest stars in the ASAS-04/08 fields and in the fields of our other objects (about 30 stars in total) and inspected them for variability. Instrumental magnitudes were corrected for the at-

[2] Our reduced Keck I/HIRES spectra of ASAS-04 and ASAS-08 are available upon request. The raw corresponding CCD frames are also available in the KOA archive of the Keck I/HIRES spectra.

[3] *IRAF* is written and supported by the *IRAF* programming group at the National Optical Astronomy Observatories (NOAO) in Tucson, AZ. NOAO is operated by the Association of Universities for Research in Astronomy (AURA), Inc. under cooperative agreement with the National Science Foundation. http://iraf.noao.edu/

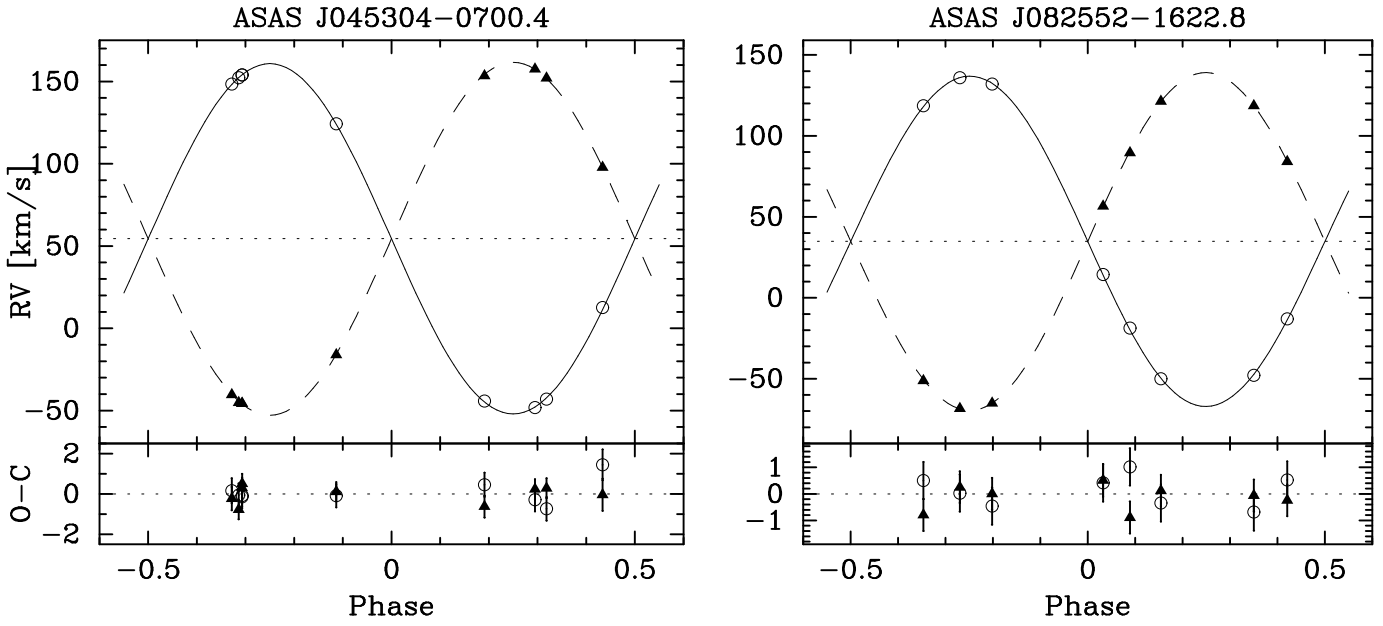

Fig. 1. Radial velocities of ASAS-04 (left) and ASAS-08 (right) from our Keck spectra together with the corresponding best-fitting radial velocity (RV) models. The RVs of the primaries are plotted with open circles and those of the secondaries with triangles. The solid line shows the best fit for the primaries and the dashed line that for the secondaries. The dotted line shows the systemic velocity γ.

mospheric extinction and compared with data from catalogues such as Tycho-2 (Hog et al. 2000), USNO-A2.0 (Monet et al. 1998), 2MASS (Cutri et al. 2003), SDSS (Abazajian et al. 2009), CMC14 (CMC 2006) and ASCC-2.5 V3 (Kharchenko 2001; with updates). Whenever possible, we converted the catalogue entries for a given star to the standard Johnson's V band, $B - V$ colour or Johnson-Cousins $V - I$ colour. When only $B - V$ was possible, we transformed it to $V - I$ with colour-colour relation for dwarfs given by Caldwell et al. (1993). Average values of V and $V - I$ from three and up to six different measurements were taken and used to transform our instrumental magnitudes to the standard ones. The *rms* of the transformation was about 0.05 mag in both bands, which later led to systematic errors in the binaries' parameters (see next section). Altogether, we collected about 440 measurements in V and 420 in I for ASAS-04 and 690 in V and 720 in I for ASAS-08. The *rms* of the final fit (see next sections) is 7 mmag in V and 9 mmag in I for ASAS-04 and for ASAS-08 6 and 8 mmag in V and I respectively. The SAAO light curves are shown in Figs 2 and 3. Differential light curves are also available on-line in the electronic version of the article.

Table 2. Orbital parameters of ASAS-04 and ASAS-08

	ASAS-04		ASAS-08	
Parameter	Value	±	Value	±
P [d]	1.62221933	2.7e-7	1.528488572	5.4e-8
T_0 [JD-2450000]	1871.16139	3.4e-4	1869.19935	1.4e-4
K_1 [km s^{-1}]	106.47	0.23	101.96	0.33
K_2 [km s^{-1}]	107.21	0.20	104.29	0.29
γ_1 [km s^{-1}]	54.54	0.21	34.94	0.25
$\gamma_2 - \gamma_1$ [km s^{-1}]	-0.33	0.29	-0.26	0.33
q	0.9931	0.0029	0.9777	0.0042
$a \sin i$ [R$_\odot$]	6.853	0.010	6.233	0.013
e	0.0	(fix)	0.005	0.002
ω[°]	—	—	84.0	6.0
$M_1 \sin^3 i$ [M$_\odot$]	0.8226	0.0024	0.703	0.003
$M_2 \sin^3 i$ [M$_\odot$]	0.8170	0.0024	0.687	0.003

Note: Values of P, T_0, e, and ω for both systems are taken from the combined spectroscopic and photometric analysis performed with PHOEBE.

4. Analysis

4.1. Spectroscopic orbits

Our first step in the analysis was to obtain a preliminary orbital solution with RV measurements independent of the light curve. We used a simple procedure that fits a double-Keplerian orbit and minimizes the χ^2 function with a Levenberg-Marquardt algorithm.

At the beginning we set all parameters free, in particular the orbital period P, time of minimum (phase = 0) T_0, eccentricity e, argument of periastron ω and systemic velocities γ_1 and γ_2 calculated for every component separately. In both binaries γ_1 and γ_2 occurred to be indistinguishable. Hence later we kept the difference between them fixed to 0. For ASAS-04 we also found e to be much less different from 0.0 than its uncertainty, so we also kept it fixed to 0 later. However, for ASAS-08 we found $e = 0.005 \pm 0.003$. Hence we left this parameter free in further analysis, also when light curves were used (see Sect. 4.3). The error value is only the formal one and it is possible that the orbit is exactly circular. Nevertheless, a non-zero eccentricity orbit better fits the observations than one with $e = 0$ and in particular allows one to better reproduce the moments of eclipses, which seem to be different from 0 and 0.5 phases. For the definition of the zero-phase – T_0 – we follow the same convention as in Hełminiak et al. (2009) according to which if $e > 0$, the moment T_0 does not coincide with any of the eclipses (see: Hełminiak et al. 2009 and references therein).

The final set of spectroscopic orbit parameters is given in Table 2. Values of the period and zero-phase as well as e and ω for ASAS-08 are from the combined RV + LC analysis. We did not include the data of Montes et al. (2007) for ASAS-08. Still, our solution is quite consistent with theirs. The model RV curves

based on the parameters from Table 2 are plotted in Fig. 1 together with the measurements. The resulting *rms* for ASAS-04 was 0.60 km s^{-1} for the primary and 0.44 km s^{-1} for the secondary and for ASAS-08 – 0.60 and 0.51 km s^{-1} for the primary and secondary respectively. TODCOR allowed us to estimate the flux ratio of binaries' components in the iodine lines regime, which is similar to the *V* band. We obtain $F_2/F_1 = 0.72 \pm 0.12$ for ASAS-04 and 0.75 ± 0.11 for ASAS-08.

Finally, we verified the quality of the best-fitting orbital RV solution in several ways. First, we carried out the tomographic disentangling of the component spectra and used them with our own procedure of computing RVs (for more details see: Konacki et al. 2010). This way we obtained sets of RVs characterized by best-fit *rms* that was a bit worse (by few 100 m s^{-1}) but the resulting best-fitting orbital parameters were consistent with those based on TODCOR derived RVs at the level of 1 sigma. Second, we carried out a bootstrap (where ∼30% of measurements are duplicated by drawing the trail RV data points with replacement from the original data sets) estimate of the parameters' errors and obtained nearly the same errors as those from the least-squares formalism, which indicates a good quality of the orbital solution from the χ^2 minimalization. One should also keep in mind that the orbital RV fit was carried out simultaneously for both components with P, T_0, e, ω and γ common for both stars, so the effective number of datapoints (measurements) is twice the number of observing epochs. Furthermore, to estimate the possible influence of systematic errors on the orbital parameters, we carried out a Monte-Carlo analysis and found that for any derived parameter the systematics are at least one order of magnitude smaller than formal uncertainties. Also, maxima in the cross-correlation function were well separated, hence we do not expect that our, favored in these cases, TODCOR based RVs could possibly lead to an orbital solution that is biased in any way as was discussed by Southworth & Clausen (2007).

4.2. ASAS-04's spotted light curve

The light curve modelling was done in two steps with two different codes. The first one – JKTEBOP (Southworth et al. 2004a,b), based on EBOP (*Eclipsing Binary Orbit Program*; Popper & Etzel 1981; Etzel 1981) – fits a simple geometric model of a detached eclipsing binary to a single light curve. The procedure is very fast, and stable and provides an extensive set of error-estimate algorithms, but is only suited to relatively well separated binaries (such as the two researched here), works with only one light curve at a time and does not allow for spots. Nevertheless, with JKTEBOP we derived quite accurate values of the parameters, which were later incorporated into the second code – PHOEBE – to obtain a full model of the system based on the two light curves and RVs. We also concluded that for both binaries the preliminary results from the two bands treated separately agree well and that the analysis performed simultaneously on two light curves is sufficient.

The *PHysics Of Eclipsing BinariEs* (PHOEBE; Prša & Zwitter 2005) code is an implementation of the Wilson-Devinney (WD) code (Wilson & Devinney 1971; with updates), which uses the computed gravitational potential of each star to calculate the surface gravity and effective temperatures. It also includes theoretical Kurucz model atmospheres to determine the radiative properties of stellar discs. It may work with several different light curves and RV curves (one or two) at the same time. We used it to obtain the final model of the ASAS-04 system. The values of some fundamental constants, like the gravitational constant or the Sun's radius, are slightly different in JKTEBOP

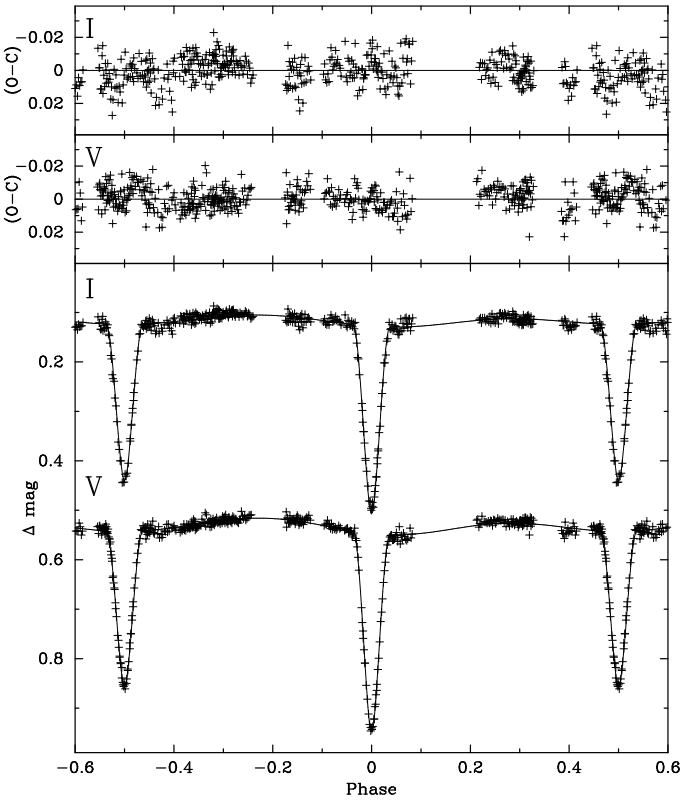

Fig. 2. ASAS-04 light curve in *V* and *I* band phase-folded with the best-fitting orbital period $P = 1.62221933$ d. The lower panel shows (artificially shifted) model light curves together with the data points obtained from the 1.0-m Elizabeth telescope. The two upper panels show the residuals from the best fit. An out-of-eclipse variation is clearly visible.

Table 3. Absolute physical parameters of ASAS-04

ASAS-04	Primary		Secondary	
Parameter	Value	±	Value	±
inclination [°]	84.60 ± 0.03			
a [R$_\odot$]	3.430	0.008	3.454	0.008
Mass [M$_\odot$]	0.8452	0.0056	0.8390	0.0056
Omega-potential	9.130	0.025	9.202	0.026
Radius [R$_\odot$]	0.848	0.005	0.833	0.005
log g	4.503	0.005	4.515	0.005
v_{syn} [km s^{-1}]	26.43	0.15	25.95	0.15
$V - I$ [mag]	0.830	0.135	0.894	0.150
Parameters of spots:				
Longitude [rad]	3.14	0.04	2.77	0.04
Latitude [rad]	0.85	0.06	1.0	0.1
Radius [rad]	0.71	0.02	0.72	0.02
% of surface	12.1	0.4	12.4	0.7
Temperat. fraction	0.975	0.002	0.967	0.002
Including spots:				
Effect. temperat. [K]	5324	200	5105	200
M_{bol} [mag]	5.46	0.16	5.68	0.17
M_V [mag]	5.64	0.23	5.92	0.25
distance [pc]	148 ± 5			
Spots rectified:				
Photosph. temperat. [K]	5340	200	5125	200
Temperature ratio	0.960 ± 0.004[a]			
Luminosity [log(L$_\odot$)]	-0.278	0.065	-0.365	0.068
M_{bol} [mag]	5.45	0.16	5.66	0.17
M_V [mag]	5.62	0.22	5.90	0.24

[a] The temperature ratio's uncertainty does not include the uncertainty in the absolute photometric calibration because it is dependent on the eclipse depths related only to the relative photometry.

and PHOEBE, so one has to be careful when incorporating the results from one code into the other one.

With PHOEBE, preparing a spotted binary model is relatively easily. This software in generally one to add many single spots on both components and fit for their size, position and temperature as a fraction of the photospheric temperature of the star[4].

First of all, we improved P and T_0 from the spectroscopic solution, after we had the photometric data and preliminary parameters from JKTEBOP. This was possible thanks to the PHOEBE's ability of working on several light curves and both RV curves simultaneously. Later, we kept them fixed and fitted for temperatures, gravitational potentials, inclination and quantities obtained from the spectroscopic orbit. Spots were added later "manually" by putting their parameters and inspecting the light curve by eye. The light curve mimics ellipsoidal variations, but a model with two spots, one on each component, both seen around eclipses, better fits the observations. If the shape of the variation were caused by tidally distorted stars, their radii would be much larger and thus eclipses would be much wider. Also, a closer inspection reveals an asymmetry between the out-of-eclipse variations.

In the last stage of modelling we set all parameters free once again to let them converge onto their final values. In our analysis we used the square-root limb-darkening law (Diaz-Cordovez & Gimenez 1992) with the coefficients automatically interpolated by PHEOEBE from the van Hamme LD tables (van Hamme 1993). The albedos for both components were held fixed at the value of 0.5 as is appropriate for convective envelopes. The gravity brightening coefficient was set to 0.32 – the classical value obtained by Lucy (1967).

It is common knowledge that it is hard to reliably estimate temperatures of eclipsing binary components. The depth of the eclipse depends not only on temperatures, but also inclination, stellar radii and the spots' configuration, and the ratio of the eclipse depths can give only the ratio of effective temperatures. Thus, to compute the stars' temperatures precisely, one must have very precise starting values. PHOEBE enables one to separately compute the flux from every component in every band. with the V and I light curves, we computed the $V - I$ colour for each star and used them with the empirical colour-temperature calibration from Casagrande et al. (2006). In this way we obtained a starting point for the temperature fitting. This presumably should have produced reliable values of the temperatures with relatively small formal errors, typically about 50 K. The idea that lays behind this approach is described by Prša & Zwitter (2005, 2006) or Kallrath & Milone (2009) and is based on the calculation of the so called *binary effective temperature* – a time- or phase-dependent value that can be associated with a colour index of the whole system (that is why two or more light curves are required). The discussion however does not include the influence of systematic uncertainties (see below) or spots. The method itself is known but was not widely used on spotted systems, which is why more attention at this point is required. However, the biggest contribution to the final error budget of temperatures in our case comes from the imperfect absolute magnitude calibration. The uncertainty of $V - I$, at the level of 0.07 mag, led to an error of about 200 K in every component's temperature. One should keep in mind that this is actually the uncertainty of the absolute scale of temperatures, while the ratio is very well constrained. We noticed that a change of any component's temperature by 5-10 K results in an eclipse depth variation that is noticeable with our photometry. We also noticed that temperature variations at a level of about 200 K have a small influence on the derived radii and increase their final uncertainties by about 25 per cent (from 0.004 to 0.005). Additionally, note that the $V - I$ colour does not change significantly even when one uses completely improbable starting values of the temperatures for the fitting.

The final set of absolute physical and radiative parameters is listed in Table 3. We managed to obtain a very good level of precision in masses and radii (about 0.6%). The resulting flux ratio in the V band is 0.790 ± 0.015, which agrees with the value from TODCOR, but is more accurate. $(V - I)$ values are corrected for the reddening (see below). Note that the absolute values and their uncertainties were not taken from PHOEBE, but were calculated by a procedure called JKTABSDIM, which is available together with JKTEBOP. It provides photometric properties (like absolute magnitudes) and distances by calculating M_{bol} on the basis of temperature, applying various bolometric corrections (Bessel et al. 1998; Flower 1996; Girardi et al. 2002) to calculate absolute magnitudes in the required bands and to compare them with the observed values to estimate the distance.

Absolute bolometric and V magnitudes were calculated with JKTABSDIM in two cases: with and without spots. In the first case we follow the concept presented by López-Morales & Ribas (2005) and calculate a value that we name an *effective temperature* – T^S_{eff}, which is actually a temperature related to the true luminosity through the Stefan-Boltzman law:

$$L \sim \sigma (T^S_{eff})^4. \tag{1}$$

Spotted areas of the stellar surface emit less radiation than "clean" photosphere, thus T^S_{eff} is not equal to the photospheric temperature – T_{phot}. The effective temperature is actually the temperature of a homogeneous, spherical blackbody of the same size as the spotted star and radiating the same amount of light as the star with a given photospheric temperature and a spot with given parameters. It can be calculated from the relation:

$$T^S_{eff} = \left[1 - 0.5\,(1-\tau^4)(1-\cos\theta)\right]^{1/4} T_{phot}, \tag{2}$$

where $\tau = T_{spot}/T_{phot}$ is a fraction of the temperature of the spot surface to the stellar photosphere temperature and θ is an angular radius of the spot (López-Morales & Ribas 2005). The spot parameters obtained from our fit are listed in Table 3. In PHOEBE the longitude of the spot is counted counter-clockwise from 0 to 2π, and 0 means the direction towards the other star. The latitude is counted from 0 (the $+z$ pole) to π (the $-z$ pole).

Using T^S_{eff} we can mimic the "apparent" properties of the components, mainly absolute V magnitudes, and compare them to observed ones. Thus we can estimate the distance. We used the parameters from Table 3 and found the distance of 148 ± 5 pc as a weighted average of eight separately calculated results, based on bolometric corrections mentioned earlier and in five bands – our (observed) V and I, and J, H, and K_s from 2MASS. The best consistency between results from various bands was reached for $E(B-V) = 0.13$. The values of the apparent M_{bol} and M_V are given in Table 3 in the *"icluding spots"* part.

We ran JKTABSDIM a second time with the photospheric temperatures T_{phot} as derived directly by PHOEBE. This way we can calculate the "true" values of M_{bol} and M_V as if there were no spots at all. They are more useful for comparison with theoretical models. We list them in Table 3 in the *"spots rectified"* part. Note that the values "with" and "without" spots are

[4] Not to be mistaken with the effective temperature. See the explanation for Eq. 2.

very close. Nevertheless, we decided to use the "rectified" ones in our further evolutionary status analysis and also the age determination, because models are calculated for unspotted stars. One should remember that the total large uncertainties in colour, temperatures, and magnitudes are caused by the error in the absolute magnitude calibration. Formal errors dependent on the quality of the photometric data are several times lower. It is particularly important for the temperature ratio which is derived with about 0.4% uncertainty.

In order to check how the potentials (thus radii) are affected by the calibration uncertainty, we set the temperatures to be higher by about 200 K, keeping their ratio constant. We held the resulting temperatures fixed (at about 4550 and 4290 K) and repeated the fit. The resulting potentials in this model have not changed significantly (well below their uncertainties), therefore we concluded that this systematic error in the photometric calibration, colour, and temperatures does not affect our final results for the radii. We made the same conclusion after lowering the temperatures by 200 K from their best-fitting model values. However, to obtain conservative radii uncertainties, we incorporated the difference in the radii between those models into the total error of the radii.

For the spot parameters, the temperature fraction and spot's angular radius are generally degenerated and it is difficult to fit them simultaneously. Some weak constrains are possible if the spot is eclipsed – from the eclipse's shape, and during the phases when the spot starts to be visible (larger spots are visible longer). For of ASAS-04 (and ASAS-08 as well) we are not able to solve that problem, consequently our solution is degenerated. Errors given in Table 3 are formal only and are probably underestimated. In our analysis, it is more important to deduce the influence of the spot on the total flux.

Figure 2 depicts our model light curves and SAAO measurements. One can easily see the out-of-eclipse variations in the system. According to our results, ASAS-04 consists of two slightly inflated stars. Theoretical models of the main-sequence stars of these masses predict radii around 0.74 R$_\odot$ (Baraffe et al. 1998). Also the temperatures exceed the values expected for main-sequence dwarfs of given masses by over 200 K for both components (e.g. Harmanec 1988; Tokunaga 2000) and indicate a ~G8 type for the primary and ~K1 for secondary (Tokunaga 2000). This may indicate a main sequence turn-off stage, which is a unique feature among known low-mass eclipsing binaries. The quite large difference in the eclipses' depths observed in our light curve, especially in the V band, implicates the temperatures ratio to be significantly different from 1. One may find it surprising, considering the nearly equal masses of the ASAS-04 components. This cannot be fully explained by the age and the evolutionary status of the system.

4.3. ASAS-08: large spots and a third light

The analysis of the ASAS-08 light curve was similar to ASAS-04's. The light curve of ASAS-08 based on our SAAO data is shown in Fig. 3. One can see that the out-of-eclipse variation is clear and pronounced. To make the fitting easier and more reliable and the model more accurate, we decided to fit a two-spot model with one spot on each component. One large spot could not explain the modulation.

As previously, we firstly corrected the ephemeris and orbital values by joining the RVs and two light curves in PHOEBE (the resulting values are given in Table 2) and then, keeping them fixed, obtained preliminary values of the temperatures and potentials. The minimal eccentricity manifests itself in phases of

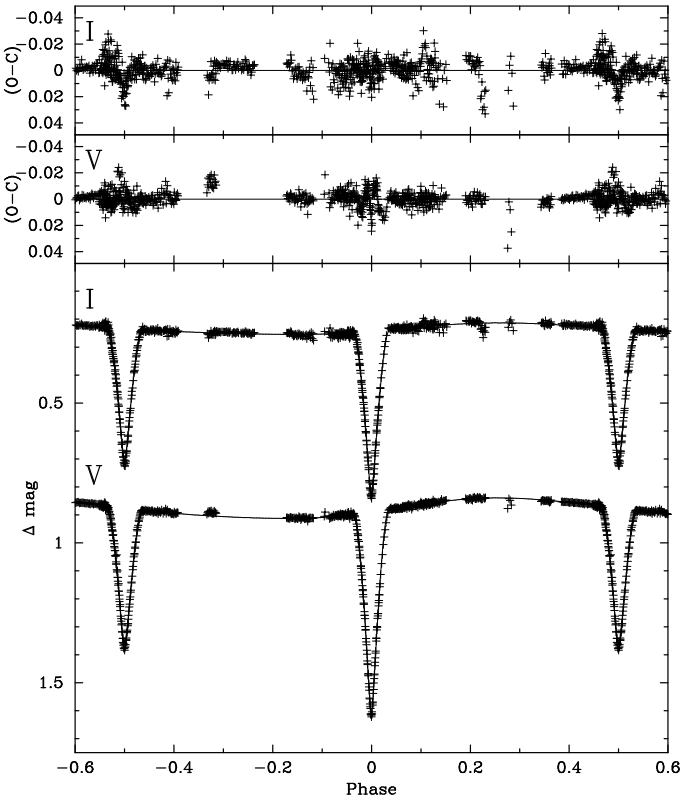

Fig. 3. Same as Fig. 2 but for ASAS-08 and its best-fit orbital period $P = 1.52848715\,d$. The variation between eclipses comes from two large, cold spots.

Table 4. Absolute physical parameters of ASAS-08

ASAS-08	Primary		Secondary	
Parameter	Value	±	Value	±
inclination [°]		89.02 ± 0.13		
a [R$_\odot$]	3.082	0.010	3.152	0.009
Mass [M$_\odot$]	0.703	0.003	0.687	0.003
Omega-potential	9.96	$^{-0.12}_{+0.06}$	9.72	$^{-0.12}_{+0.15}$
Radius [R$_\odot$]	0.694	$^{+0.007}_{-0.011}$	0.699	$^{+0.011}_{-0.014}$
log g	4.600	0.016	4.585	0.016
v_{syn} [km s^{-1}]	22.9	0.4	23.1	0.4
$V - I$ [mag]	1.26	0.11	1.40	0.11
Parameters of spots:				
Longitude [rad]	1.70	0.08	3.35	0.15
Latitude [rad]	0.30	0.02	1.3	0.3
Radius [rad]	1.55	0.02	0.83	0.08
% of surface	49	1	16	3
Temperat. fraction	0.943	$^{-0.005}_{+0.004}$	0.986	$^{-0.005}_{+0.002}$
Including spots:				
Effect. temperat. [K]	4230	200	4080	200
M_{bol} [mag]	6.87	0.21	7.03	0.24
M_V [mag]	7.58	0.40	7.92	0.45
distance [pc]		44 ± 9		
Spots rectified:				
Photosph. temperat. [K]	4350	200	4090	200
Temperature ratio		0.940 ± 0.004[a]		
Luminosity [log(L$_\odot$)]	-0.808	0.082	-0.909	0.087
M_{bol} [mag]	6.78	0.20	7.02	0.22
M_V [mag]	7.44	0.35	7.90	0.40

[a] The temperature ratio's uncertainty does not include the uncertainty in the absolute photometric calibration because it is dependent on the eclipse depths related only to the relative photometry.

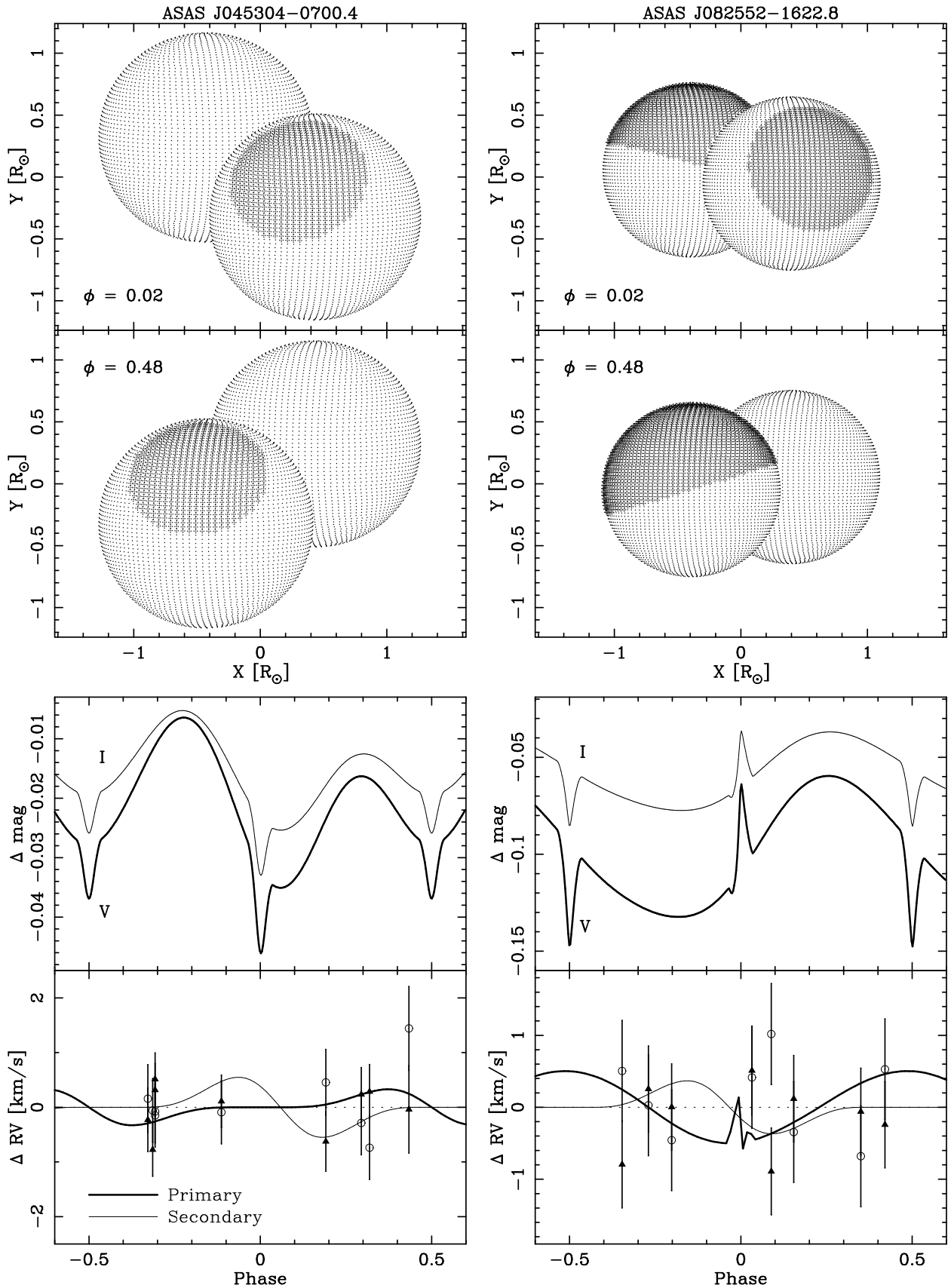

Fig. 4. Spots on researched systems. *Top:* 3D reconstruction of ASAS-04 (left) and ASAS-08 (right) during the primary ($\phi = 0.02$) and secondary eclipse ($\phi = 0.48$). Units are solar radii, scale is the same for both systems; *bottom:* Influence of spots on the ASAS-04 and ASAS-08 light and RV curves. The absolute difference between a spotted and non-spotted case is plotted. Differential RV curves are overplotted on RV residuals, the same as in Fig. 1.

Table 5. Parameters of the third light in the ASAS-08 solution.

Parameter	Value	±
% of flux in V	10.0	—
% of flux in I	17.0	1.2
$V - I$ [*mag*]	1.97	0.24
M_V [*mag*]	9.40	0.52

brightnes minima, which for ASAS-08 are $\phi_{prim} = -0.00018$ or 0.99982 and $\phi_{seco} = 0.50018$. Spots were added later "manually" by putting in their parameters and inspecting the light curve by eye. The automatic fitting procedure was run only when the initial model was reproducing the light curve shapes in a satisfying way. From the character of the brightness variation, we deduced that the spots should be relatively large and reach the polar regions, at least for one component. As for ASAS-04, the solution is degenerated for spot sizes and temperature factors.

The last stage was adding the third light into the solution. We aimed to keep the flux ratio in V unchanged at the level given by the *Hipparcos* photometry and Montes et al. (2007) data (see Sect. 2.2), but we had no constrains for the I band. Unfortunately, PHOEBE does not allow to fix the third light in one band and fit for it in the other at the same time. Hence we decided to find several light curve solutions for a range of the I band third light contamination values and compare their quality. Temperatures, potentials, inclination and, spot parameters were fitted while the third light flux was held fixed. The quality criterion was based on the χ^2 for both light curves, shapes of the model curves and the soundness of the obtained parameters.

We found that some parameters, especially the radii, varied significantly with the third light level in I. Above a certain value, the resulted R_1 started to be smaller than R_2, which is somewhat improbable when the binary is on the main sequence. When the third I flux level was too low, we ended up with a situation where the third component is hotter (smaller $V - I$) than the binary components. If that is the case, and if it is gravitationally bound to ASAS-08, as suggested by Montes et al. (2007), one should expect it to be brighter in V than the binary. We could also reject some solutions by inspections of model light curves, which for example did not reproduce the depth of one of the minima. Finally, we found that when we increased the third I flux, the χ^2_V minimum (for the V curve) was getting lower, while χ^2_I (the I curve) was increasing. The final level of the third light contamination in the I band – 17% – was found to be a minimum of the sum $\chi^2_V + \chi^2_I$ and occurred to be a compromise between all previously mentioned constrains. Still the resulting R_1 is smaller than R_2, but within errors we are able to find $R_1 > R_2$.

Tables 4 and 5 show the full set of results of our modelling. In Table 4 we collected stellar absolute physical parameters (as in Table 3 for ASAS-04). The resulting flux ratio in V band is 0.68 ± 0.01, which agrees with the value from TODCOR, but is more accurate. We reached 0.43% precision in masses and 1 – 2% precision in radii. Most of the errors are caused by the third light I flux's uncertainty. The formal error of modified potentials is at the level of 0.04 and the rest is the contribution from the third light. As for ASAS-04, changing temperatures by 200 K did not affect the potentials significantly. Uncertainty in the absolute photometric calibration was however added to the colour and the absolute magnitudes error. Absolute bolometric and V magnitudes were again calculated with JKTABSDIM for the two cases with and without spots. In the case with spots, we found the distance to ASAS-08 to be 44 ± 9 pc, which agrees very well with the one from *Hipparcos* (45.8 ± 4.7 pc). On this basis, we also calculated M_V for the third star. Its uncertainty given in Table 5 includes the *Hipparcos* measurement error, which is however not incorporated into the $V - I$ error because the colour is calculated straightforwardly from the model. The error of the absolute photometric calibration is added to both mentioned parameters. We also note that values of M_{bol} and M_V for the binary's components are again consistent within error bars but, as for ASAS-04, we decided to use the "rectified" ones in further analysis.

In order to show the influence of spots in both investigated systems quantitatively, in we plot Figure 4 the absolute difference in magnitudes between our final models and models of binaries with the same absolute physical parameters but without spots. Additionally we plot differential RV curves constructed with PHOEBE as a difference between the spotted and unspotted model with the eclipse proximity effects turned off in both cases so that the Rossiter-McLaughlin effect is not shown. One can deduce that for ASAS-08 a spotted surface is seen all the time because the spot on the primary covers the polar region. The magnitude of the light variation – 0.03 – 0.05 – is not very high. It is in deed lower than the peak-to-peak scatter of the ASAS measurements, so from the ASAS data only it would be difficult to deduce the presence of spots in our systems. Especially if the spots were moving during the nine years of observations, which is presumably possible. For this reason our RV measurements could have been obtained when the spot configuration was different. We cannot say much about the spot's pattern at the moment of spectroscopic observation. From the Fig. 4 we can however estimate that the RV curve's modulation is smaller than about 0.5 km s^{-1} for the observed configuration of spots in our photometric data set. Obviously, this is within the total RV errorbars. We also found that turning on the proximity effects while fitting to RVs in PHOEBE does not significantly change the results and in the case of ASAS-08 makes the *rms* of the RV fit a bit larger. We believe the total error of the RV measurements does account for the overall activity of the targets and therefore the resulting uncertainties of the best-fitting parameters are realistic.

Figure 4 also shows three-dimensional reconstructions of ASAS-04 and ASAS-08 in two phases – $\phi = 0.02$ (primary eclipse) and $\phi = 0.48$ (secondary eclipse). Values on axis are solar radii and stars are shown on the same scale.

The properties of the spots can be found to be slightly puzzling. Among several late-type detached eclipsing binaries known to have spots, for example CM Dra (Lacy 1977; Morales et al. 2009a), YY Gem (Kron 1952; Torres & Ribas 2002), CU Cnc (Ribas 2003), GU Boo (López-Morales & Ribas 2005), LP 133-373 (Vaccaro et al. 2007) or BD -22 5866 (Shkolnik et al. 2008), none is reported to be covered to an extent such large as ASAS-08. Some of seven eclipsing binaries listed by Coughlin & Shaw (2007) have more than half of their surface covered by spots, but their real masses are only estimated from the evolutionary models. In some other cases, like GU Boo (López-Morales & Ribas 2005), the temperature factor is higher than 1 (a "bright" spot). It is not clear if the existence of such a feature is physically valid, but an explanation given by López-Morales & Ribas (2005) suggests that almost whole star's surface is covered by many small spots of high contrast and only a small fraction of "clear" photosphere is seen. This seems to be the case of ASAS-08 as well especially having the temperature factors close to 1.

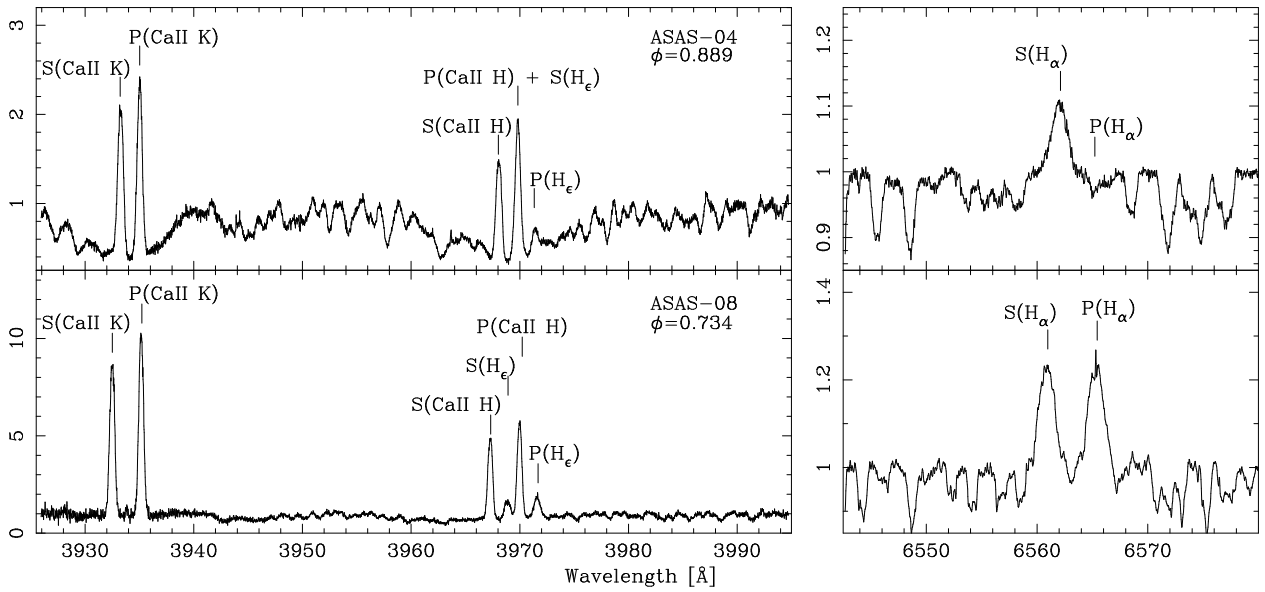

Fig. 5. Portions of continuum-normalized spectra of ASAS-04 (top) and ASAS-08 (bottom) around Ca II K and H (left) and H$_\alpha$ (right) lines with marked emission features. The primaries features are labelled with P(...) and the secondaries with S(...). For ASAS-04 the primary's Ca H line is blended with the secondary's H$_\varepsilon$. Both spectra were taken on October 12, 2005. Orbital phases are labelled.

5. Age determination and evolutionary status

5.1. Activity and kinematics

As mentioned above, radii of both ASAS-04 components and their higher temperature indicate late main-sequence or even a post-main-sequence evolutionary stage. Inflated radii are commonly observed in low-mass eclipsing binaries, but together with lower temperatures (Torres & Ribas 2002; Chabrier et al. 2007), which for ASAS-04 seem to be higher than predicted. This may still be the effect of the absolute magnitude calibration, but it would mean that the real temperatures differ by almost 3σ. Keeping in mind the uncertainty in the temperatures one cannot be convinced that ASAS-04 is indeed an old system. But other observational facts seem to support this hypothesis. Young objects of this mass should exhibit quite a high level of activity. A substantial emission in X-rays and UV should be observed and a strong emission in spectral lines should also be present. No significant UV emission is seen around ASAS-04's position, and at a distance of 13" a faint X-ray source can be found – 1RXS J045304.1-070011. López-Morales (2007) found a correlation between the activity level and radii of low-mass stars in close binaries. The fractional deviation of a star's radius as compared to 1 Gyr, $Z = 0.02$, $\alpha = 1.0$ BCAH98 isochrone (Baraffe et al. 1998) for main-sequence stars turned out to be a function of the X-ray-to-bolometric luminosity ratio – L_X/L_{bol}. For a linear correlation of L_X and rotational velocity (as found by Fleming et al. 1989), and stars $M < 0.7$ M$_\odot$, the relation was

$$\frac{R_{obs} - R_{mod}}{R_{mod}} \propto 74.43 \frac{L_X}{L_{bol}}, \tag{3}$$

where R_{obs} is the observed radius and R_{mod} is the radius predicted by the BCAH98 isochrone for a given mass. When stars with $M > 0.7$ M$_\odot$ were included, the slope changed to 62.511 (López-Morales 2007). The uncertainties of the slope's values were not given, nor was the zero-point of the relation, but from Fig. 3. in López-Morales (2007) one can deduce that it was about 0.005 and 0.015 for the cases without and with the more massive stars respectively.

For the ASAS-04 we found $(L_X/L_{bol})_1 = 7.0 \pm 2.5 \cdot 10^{-4}$ and $(L_X/L_{bol})_2 = 8.4 \pm 3.0 \cdot 10^{-4}$ which corresponds to 5 and 6% excess of the radii on the main sequence respectively. Our measurements indicate 13.0 ± 0.7% for the primary and 11.7 ± 0.6% for the secondary, which disagrees with the relation even when the large scatter of the López-Morales (2007) data points is taken into account.

In the spectra of ASAS-04 we detected a weak emission in H$_\alpha$ for the secondary component and for the primary the absorption line is almost filled-in. In terms of H$_\alpha$ equivalent width (see below) we can consider ASAS-04 as "weakly active". However, we also detected a substantial emission in the Ca II H and K lines, as well as H$_\varepsilon$. Balmer line H$_\beta$ was in the region between "blue" and "green" chips of the HIRES detector, so it could not be subtracted. Marks of emission in H$_\delta$ and H$_\gamma$ can also be found, but blending with other lines made them too difficult to measure. No emission was found in helium lines (4027, 4473, 5877 and 6678 Å) or in the Na I D$_1$ and D$_2$ lines, which suggests no variability in the lower chromosphere (Montes et al. 1997). We list the equivalent widths given in Åfor all emission lines measured in Table 6. Portions of spectra around H$_\alpha$ and Ca II lines are depicted in Fig. 5. The clear existence of some activity indicators is nevertheless not surprising. Recent results for low-mass detached eclipsing binaries suggest that the stellar activity is excited by the presence of a close companion (see e.g. López-Morales 2007), and the presence of spots is quite common among those objects. A recent spectroscopic research by Parihan et al. (2009) revealed that the H_α emission is probably variable. Their low-resolution spectra show only filled-in lines and no emission components at the level similar to the one presented here.

In order find additional clues that point to ASAS-04 as an old object, we also calculated the galactic space velocities U, V, W[5] with regard to the local standard of rest (LSR; Johnson & Soderblom 1987). We applied our values of the radial systemic velocity and distance estimate together with the proper

[5] Positive values of U, V, and W indicate velocities towards the Galactic center, the direction of rotation and the north pole respectively.

Table 6. Equivalent widths of emission lines of ASAS-04 and ASAS-08

		ASAS-04		ASAS-08	
Line	λ [Å]	Pri.	Sec.	Pri.	Sec.
H_α	6563	0.19	-0.03	0.65	0.55
H_ε	3970	0.34	0.36	0.92	1.05
Ca II H	3968	2.02	2.12	3.17	3.66
Ca II K	3934	2.66	2.79	5.31	5.55
H_6	3889	—	—	0.4	0.4

motion of $\mu_\alpha = 12.02$ mas/yr and $\mu_\delta = -46.12$ mas/yr from the PPMX catalogue (Röser et al. 2008). Values of $U = -15.6 \pm 0.9$, $V = -43.1 \pm 1.4$ and $W = -26.1 \pm 1.1$ km s^{-1} put ASAS-04 outside of any known young moving group or group candidate (Zhao et al. 2009), being closest to the Hercules stream (Seabroke & Gilmore 2007), and at the transition area between the thin and thick galactic disc (Bensby et al. 2003; Nordström et al. 2004). Bensby et al. (2007) investigated the age and abundance of the Hercules stream and found that this feature is composed of a mixture of young and old stars, all of which show kinematic characteristics similar to the thick disc. Thus we may conclude that ASAS-04 is an old system, presumably from the thick disc. The maximal age of the thin disc is not well constrained, but all researches agree with Jimenez et al. (1998) who derived $t_{TD} > 8$ Gyr. Although this value seems to be secure for the lower limit of the ASAS-04 age, considering other facts (see next section) we adopt 5 Gyr as the lower limit. If ASAS-04 is older than 8 Gyr it would mean that it is currently close to the turn-off point and ends its main-sequence evolution, which makes it a very interesting object for more research.

On the contrary, ASAS-08 is a younger, likely a main-sequence binary. With our value of the systemic radial velocity, the *Hipparcos* distance, and the PPMX proper motion ($\mu_\alpha = -183.7$ mas/yr and $\mu_\delta = 15.49$ mas/yr) we obtained $U = -26.9 \pm 0.8$, $V = -20.6 \pm 0.3$ and $W = -18.0 \pm 1.2$ km s^{-1}. Those values put ASAS-08 exactly in the thin disc regime, but it is hard to associate the binary with any young moving group, so we can conclude that its age is more than ~ 1 Gyr. The level of activity supports this conclusion. Hawley et al. (1999) have proven that M dwarfs in young open clusters have a well defined $V - I$ colour at which their activity, measured from the H_α emission, becomes ubiquitous. Active stars (which have EW$_{H_\alpha}$ ≥ 1 Å) from a certain cluster are redder than this characteristic $V - I$. Hawley et al. (1999) gave a relation between the age t_{H_α} of the cluster and this "H_α-limit" colour at which M dwarfs have EW$_{H_\alpha} \simeq 1$ Å:

$$V - I = -6.91 + 1.05(\log t_{H_\alpha}). \quad (4)$$

Later Gizis et al. (2002) also used this relation for field M dwarfs. Both ASAS-08 components have EW$_{H_\alpha} \simeq 0.6$ Å(which agrees with Christian & Mathioudakis 2002), consequently we can estimate the lower limit for the system's age with Eq. 4. With our value of the secondary's $V - I$ we conclude that the system must be much older than 85 Myr. If we further assume that the third component is inactive, in the meaning of EW$_{H_\alpha}$, we get a lower limit for the age of the system to be about 290 Myr. As for ASAS-04, according to the definition by Hawley et al. (1999), we consider ASAS-08, as well as ASAS-04, as "weakly active" in terms of H_α equivalent width (and in those terms only). ASAS-08 was also observed by Parihan et al. (2009), who recorded substantial emission in the H_α line at a level similar to the one presented here.

Other activity indicators are also detected in emission, especially the calcium H and K lines are very strong (see Fig. 5 and Table 6). As for ASAS-04, other Balmer lines are also seen in emission, including weak H_6 (out of the range of Fig. 5). Other lines, such as sodium D or He I 5877 Å, were not found in emission, but Parihan et al. (2009) noted them to have "comparable levels of emission", which presumably may indicate their variability. This implicates the level of activity is higher than for ASAS-04 and is consistent with the presence of larger spots. Also the X-ray-to-bolometric luminosity ratio is higher than for the former system. When we incorporated the data for 1RXS J082551.4-162244 from ROSAT (Voges et al. 1999) and assumed a linear correlation between L_X and v_{rot}, we found $(L_X/L_{bol})_1 = 7.6 \pm 3.5 \cdot 10^{-4}$ and $(L_X/L_{bol})_2 = 9.5 \pm 4.0 \cdot 10^{-4}$ for the primary and secondary respectively. The excess of the radii, measured in the same manner as previously, is 8^{+1}_{-2}% and $10.5^{+2.0}_{-1.5}$% respectively. Those numbers agree within errors with the relation found by López-Morales (2007), but place ASAS-08 above it.

5.2. Isochrones

In this section we compare our results with several popular and widely used sets of theoretical evolutionary models and isochrones — Y^2 (Yi et al. 2001; Demarque et al. 2004), BCAH98 (Baraffe et al. 1998), PADOVA (Girardi et al. 2000; Marigo et al. 2008) and GENEVA (Lejeune & Shaerer 2001).

5.2.1. Inflated ASAS-04

In Fig. 6 we show the results for ASAS-04 together with several isochrones on the mass versus bolometric magnitude M_{bol}, radius R, logarithm of temperature $\log(T_{phot})$, absolute V magnitude M_V and observed $(V-I)$ colour planes. We compare our results with theoretical predictions for three scenarios: (1) the early main-sequence stage and solar composition (*left*); (2) late main-sequence stage and reduced metallicity (*middle*); (3) main sequence turn-off and solar metallicity (*right*). Because of the limited availability our sets are not uniform for the scenario (2) and (3) – slightly different metallicities were used for the GENEVA and BCAH98 sets in (2) and a different age for BCAH98 in the scenario (3). In this case we may consider this isochrone as a lower limit for the age estimate as it usually lies close to one of the errorbars. Isochrones for the scenarios (2) and (3) were selected to fit our measurements in the M/M_{bol} plane. We chose this plane as a reference since recent findings show that although radii and temperatures are not particularly well reproduced, the luminosity (hence M_{bol}) is and one can then fit an isochrone to the data if the radius is scaled by a factor β and the temperature by $\beta^{-0.5}$ (Chabrier et al. 2007; Morales et al. 2009b).

The left column clearly shows that ASAS-04 cannot be at the early main sequence stage. The observed properties are not reproduced in any of the panels, except for $M/(V-I)$. As was mentioned above, both the radii *and* temperatures exceed predictions. One could fit a 1 Gyr isochrone to our data if $Z < 0.006$ was assumed. However, considering the activity-radius relation (López-Morales 2007) and kinematics, we find this scenario very unlikely.

The degeneration between age and metallicity of models that fit the data is already well known (Lastennet & Valls-Gabaud 2002) and ASAS-04 is no exception. Our measurements of mass and M_{bol} are well reproduced not only by models from Fig. 6, but also for example for $t = 8$ Gyr, $Z = 0.012$. One can also

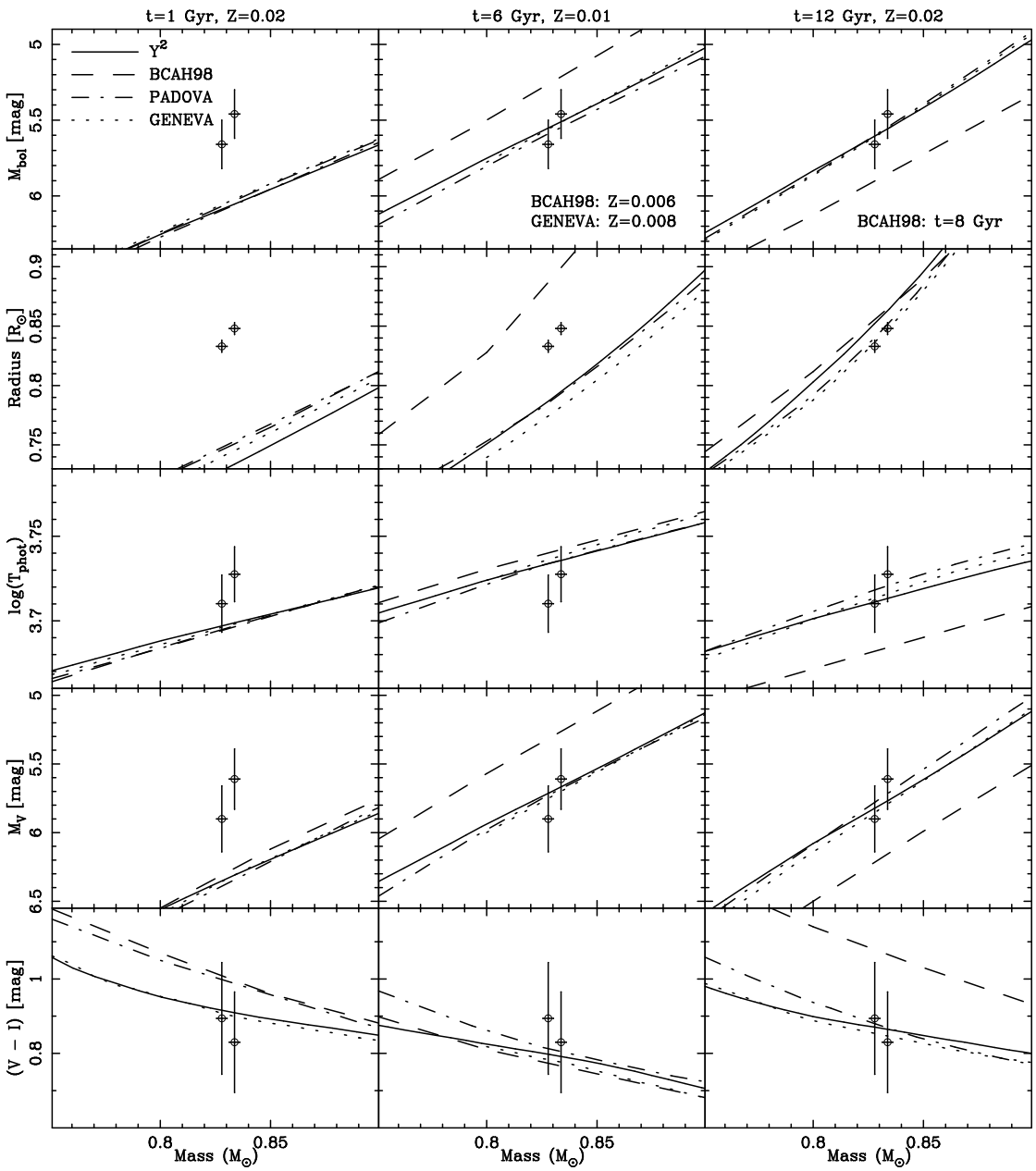

Fig. 6. Comparison of several physical parameters as a function of mass for ASAS-04 with several sets of isochrones. The left column is for the age of 1 Gyr and solar metallicity, the middle column is for 6 Gyr and metallicity below solar (0.01 for PADOVA and Y^2, 0.008 for GENEVA and 0.006 for BCAH98), the right column is for solar composition and $t = 12$ Gyr, except BCAH98 (8 Gyr). From the highest to the lowest, the rows show mass vs. M_{bol}, R, $\log(T_{phot})$, M_V and $(V - I)$ colour. The measurements and their uncertainties are taken from Table 3.

see how BCAH98 for $t = 6$ Gyr and $Z = 0.006$ varies from the other isochrones. For the presented case of $t = 6$ Gyr, we observe the aforementioned discrepancies in the radii and temperatures (except for BCAH98, which is for smaller Z). Thus we find this age/metallicity set a probable one. We observed the same behaviour but with smaller discrepancies for sets with $t = 8$ Gyr and $Z = 0.012$. For the case of 6 Gyr and $Z = 0.01$ a single correction factor $\beta \equiv R_{obs}/R_{mod}$ can be found for both components and would be $\beta \simeq 1.055$. This corresponds to the shift in $\Delta \log(T_{phot}) \simeq 0.012$, which would allow for fitting a single isochrone. The discrepancies diminish around $t \sim 10 - 11$ Gyr, where the radii and temperatures, as well as M_V and $(V - I)$ are nicely reproduced. For 12 Gyr the predicted radii start to be larger than observed, while in the other planes we obtain a good fit. Thus we consider 12 Gyr as an upper limit to the ASAS-04 age. Note also that the BHAC98 model for 8 Gyr and the solar Z predicts the largest radii of all sets, despite predicting the lowest temperatures and luminosities.

The presented models suggest that the radius and temperature discrepancies may not be significant for older stars. This seems to be supported by the recent discovery of a 0.88 + 0.86 M$_\odot$ evolved eclipsing binary V69-47Tuc in the famous globular cluster (Thompson et al. 2010). Several sets of theoretical models succeeded to fit the observed radii and bolometric luminosities of this binary components with a single isochrone. The estimated age was 11.3 Gyr and [Fe/H]=-0.70 was assumed. Considering the similar masses of the ASAS-04 components we may expect that the almost perfect fits of $t > 10$ Gyr isochrones are plausible.

From the discussion above, we can deduce the age of ASAS-04 to be 5 – 12 Gyr and the metal abundance between 0.008 and 0.02 with the ranges of 8–11 Gyr and Z from 0.012 to $\sim$ 0.018 be the most probable ones. This makes it one of the oldest low-mass eclipsing systems known to date. Recently several evolved low-mas eclipsing binaries were found in globular clusters: a 0.81 + 0.68 M$_\odot$, older than 10 Gyr OGLEGC 17 in ω Cen (Thompson et al. 2001), 0.945+0.144 M$_\odot$ system V209 in the same cluster[6] (Kałużny et al. 2007), a 12 Gyr-old, 0.79 + 0.23 M$_\odot$ binary V32 in NGC 6397 (Kałużny et al. 2008), and the already mentioned V69-47Tuc (Thompson et al. 2010). In all these cases the primary begins to evolve onto the sub-giant branch. Also a few slightly more massive systems were found to be about 10-11 Gyr old. These are: CG Cyg (0.94 + 0.81M$_\odot$; Popper 1994), RW Lac (0.93 + 0.87M$_\odot$; Lacy et al. 2005) and HS Aur (0.90 + 0.88M$_\odot$; Popper et al. 1986). ASAS-04 appears to be similar but less massive than HS Aur. Hence it appears to have the smallest masses for a rare group of late-type field eclipsing systems that come to the end of their main-sequence life.

One should keep in mind that the isochrones fit to the measurements thanks to the relatively large errorbars caused by the systematic error contribution of the absolute photometric calibration. Still, the temperature ratio and therefore the magnitude difference are constrained well and none of the models predict them correctly.

5.2.2. Main sequence ASAS-08

We show a comparison of our results for ASAS-08 with the isochrones in Fig. 7. This time we selected isochrones for ages t = 1 and 5.0 Gyr with the solar abundance (left and middle) and 10.0 Gyr and Z higher than solar. Because of the limitations of the available models, our sample is not uniform. The GENEVA set of models lacks isochrones for masses below 0.8 M$_\odot$ and $Z > 0.02$, that is why they are plotted only in two columns. Other sets are also limited in high metallicities: PADOVA has its maximal $Z = 0.03$, Y[2] are plotted for $Z = 0.04$. The BCAH98 model in the right column is prepared for the helium abundance of $Y = 0.282$ and maximal age of 8 Gyr. An isochrone with this Y reproduces properties of the Sun at its current age (Baraffe et al. 1998) and for t = 8 Gyr also fits quite nicely to ASAS-08.

As for the previous system, we select models that fit our data in the mass-bolometric magnitude plane. ASAS-08 is again a case of the degeneration between age and metallicity, but we may estimate a lower limit of Z to be about 0.012. Not much difference is seen in the main-sequence stage (between 1 and 5 Gyr in Fig. 7), but to fit an isochrone with a larger Z, one needs to go to 8 – 10 Gyr regime. For such a high age theoretical models seem to match our data quite well, but this scenario is unlikely when considering activity and kinematics. Thus a main sequence evolutionary stage of ASAS-08 is very probable.

As for most of other known low-mass eclipsing binaries, for ASAS-08 we observe clear discrepancies between the models and observations in radii and temperatures on the main sequence. Every model we compare requires a slightly different correction factor $\beta \equiv R_{obs}/R_{mod}$ and within errorbars one can find a single value of $\beta \simeq 1.09$ for both components. This corresponds to a shift of 0.02 in $\log(T_{phot})$, which allows for fitting a single isochrone.

One can notice that around $M \sim 0.7$ M$_\odot$ various sets predict significantly different $(V - I)$ colour, which is of course related to the different physics used in each model. In our case only the PADOVA and BCAH98 sets succeed to match the data within errorbars. The BCAH98 set fits slightly better for 5 Gyr while PADOVA for 1 Gyr. With those two sets and our estimates of $(V - I)$ and M_V for the third body, we can also estimate the mass of this star. In Fig. 8 we show our estimates of $(V - I)$ and M_V for all three bodies in the ASAS-08 system. For the comparison we plot all sets, and all fit within errorbars but only PADOVA and BCAH98 fit simultaneously to the mass measurements. PADOVA (dot-dashed) gives the consistent third body mass estimate for $M_3 = 0.43 - 0.5$ M$_\odot$ and BCAH98 (dashed) ends at 0.6 M$_\odot$, which in the colour/brightness plane is close to the edge of errorbars. Thus 0.6 M$_\odot$ is an upper limit of the third body's mass. These values put the third component into the late K spectral type range ($T_{eff} \sim 4000$ K as predicted by Harmanec 1988). The $V - I$ colour itself predicts a fairly later type around M2 ($T_{eff} \sim 3600$ K, based on Bessel et al. 1998). The angular distance is 0.845" (from *Hipparcos*), which corresponds to a projected separation of 39 AU if gravitationally bound. We expect that a $\sim$ 0.5 M$_\odot$ star at this distance would cause a significant perturbations in the binary, which presumably could be detected with a long-term RV or eclipse timing.

6. Discussion and conclusions

We presented an analysis of two new eclipsing systems with component masses below 1 M$_\odot$ – ASAS J045304-0700.4 and ASAS J082552-1622.8 – the first two of our sample of low-mass eclipsing binaries from the ASAS database. Both objects seem to be interesting targets for further studies: ASAS-04 because of its evolutionary status possibly at the end of the main-sequence stage and ASAS-08 because of the activity, the unusually large spot coverage and the third component. The third body may be responsible for the low but measurable eccentricity of this system's orbit.

Our mass and radius measurements (open circles) are compared with the other known low-mass eclipsing binaries in Fig. 9. We selected main-sequence systems with parameters derived with an accuracy better than 3% (open squares), as well as several systems with ages higher than about 10 Gyr (open triangles) and systems with pre-main-sequence components (crosses). A BCAH98 isochrone for t = 1 Gyr, $Z = 0.02$ and $M > 0.6$ M$_\odot$ is also shown, supplemented by a similar isochrone from Chabrier & Baraffe (1997; CB97) set, for masses below 0.8 M$_\odot$[7].

We derived both objects' absolute physical parameters with a precision of at least single %. However, uncertainties of some of the values like the temperatures can likely still be improved because their systematic errors are quite large. PHOEBE's way of calculating the temperatures based on the passband luminosities and colour-temperature calibrations (more details in Prša & Zwitter 2006) produces low formal errors, but an uncertainty coming from the photometric calibration also contributes. The absolute scale of the temperatures is uncertain, but their ratio, highly dependent on the eclipse depths, is constrained rather well. Its value for ASAS-04 seems to be too far from unity for stars of these masses. There seems to be a discrepancy between the theoretical and observed radii and temperatures for ASAS-08 and ASAS-04 if they are on the main sequence, which is common for low-mass binaries with main sequence components (see Fig. 9). But if ASAS-04 is old, the isochrones of about 10 – 11 Gyr match the measured radii, temperatures, and luminosities simultaneously.

[6] This system probably went through a common-envolope phase.

[7] We did not use this set in our analysis because its mass range does not reach ASAS-04 values.

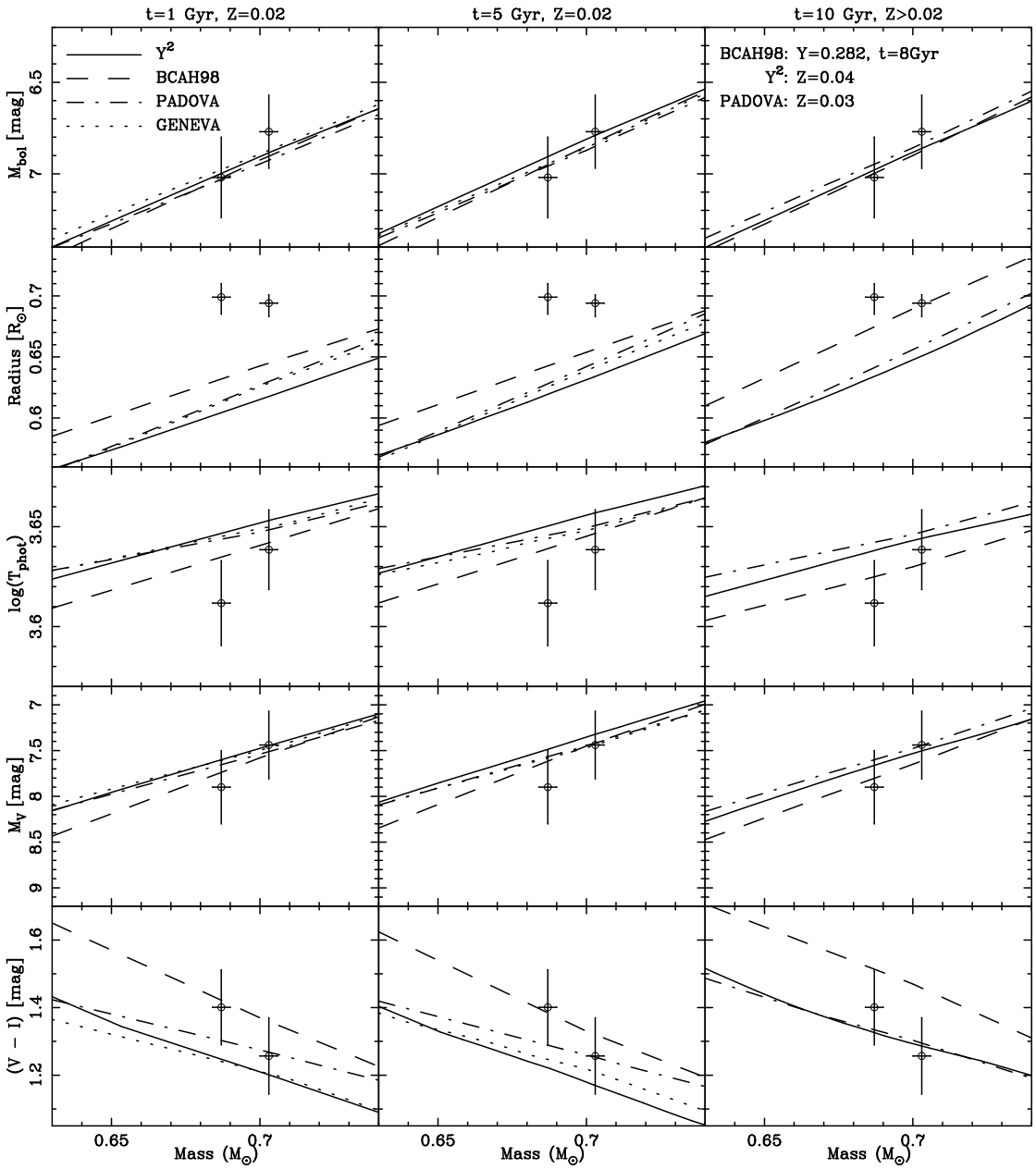

Fig. 7. Same as Fig. 6 but for ASAS-08. Different ages and metallicities were used: $Z = 0.02$ with $t = 1$ (left) and 5 Gyr (middle), and $Z > 0.02$ for $t = 10$ Gyr (right column). For the last case the GENEVA set was not available for masses below 0.8 M$_\odot$ and other sets' metallicities vary, as labeled. As for ASAS-04, BCAH98 set was available only for 8 Gyr and a helium abundance value $Y = 0.282$.

Our orbital/physical models, which predict large areas of both stars in both systems to be covered by spots are not the only possible solution to explain the light curve's shape. However, in the case of a different spot scenario, the component masses and radii should not change significantly. Nevertheless, we tried to obtain spot models as robust as possible, and the large difference in the temperatures of the ASAS-04 components appears to be real and challenges the evolutionary models. The isochrones in general succeed to reproduce the results for both systems (with the exception of ASAS-08 radii and temperatures, as expected for the main sequence, and temperature ratio in ASAS-04) and our distance estimation for ASAS-08 based on the "effective" temperatures agrees very well with the *Hipparcos* value. This supports the statement that our orbital/physical models are realistic and accurate.

Acknowledgements. We would like to thank Grzegorz Pojmański for pointing out several suitable ASAS targets in the early stages of this project. KGH would like to thank John Menzies from the South African Astronomical Observatory for his support during observations, Janusz Kałużny from the NCAC Warsaw for useful advices and Tomasz Kamiński from the NCAC Toruń for his help with spectra reduction.

The authors wish to recognize and acknowledge the very significant cultural role and reverence that the summit of Mauna Kea has always had within the indigenous Hawaiian community. We are most fortunate to have the opportunity to conduct observations from this mountain.

This work is supported by the Foundation for Polish Science through a FOCUS grant and fellowship, by the Polish Ministry of Science and Higher Education through grants N203 005 32/0449 and 1P03D-021-29.

This research was co-financed by the European Social Fund and the national budget of the Republic of Poland within the framework of the Integrated Regional Operational Programme, Measure 2.6. Regional innovation strategies and transfer of knowledge - an individual project of the Kuyavian-Pomeranian Voivodship "Scholarships for Ph.D. students 2008/2009 - IROP"

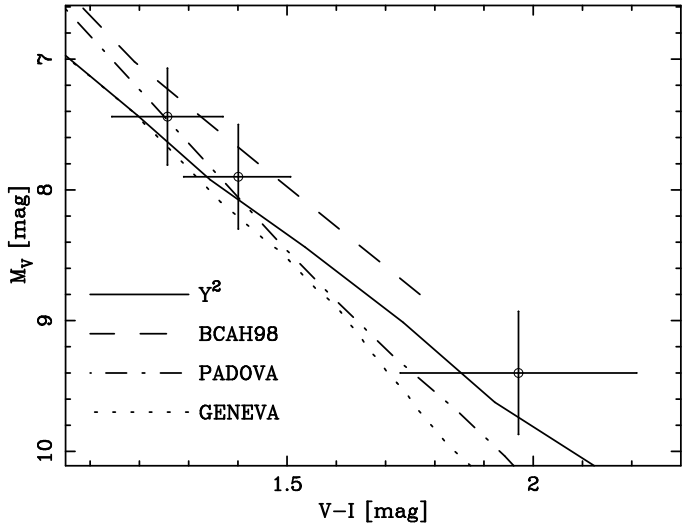

Fig. 8. $(V-I)/M_V$ plane with the theoretical isochrones of 1 Gyr and $Z = 0.02$, and our results for the three bodies in the ASAS-08 system. Data points and uncertainties are from Tables 4 and 5. The BCAH98 model ends for 0.6 M$_\odot$.

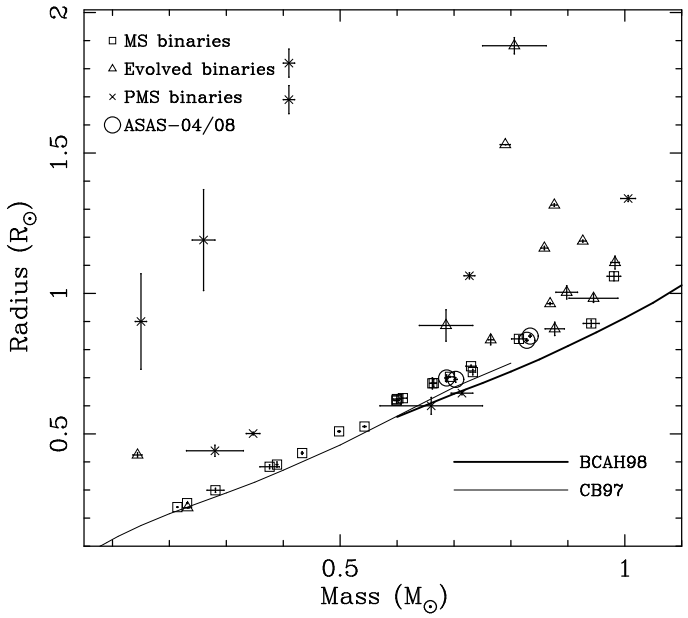

Fig. 9. Mass/radius data for eclipsing binaries with masses below 1 M$_\odot$. For main-ssequence binaries only those with M and R uncertainties below 3% were chosen from Torres & Ribas (2002); Ribas (2003); Shkolnik et al. (2008); Irwin et al. (2009); Morales et al. (2009a,b); Różyczka et al. (2009); Torres et al. (2010). Data for evolved ($t \gtrsim 10$ Gyr) systems were taken from: Popper et al. (1986); Popper (1994); Kałużny et al. (2007, 2008); Thompson et al. (2001, 2010); Lacy et al. (2005). Pre-main-sequence systems data were taken from: Irwin et al. (2007); Stassun et al. (2007, 2008); Çakırlı et al. (2009); Çakırlı& İbanoğlu (2010). The BCAH98 model for $t = 1$ Gyr and $Z = 0.02$, which ends for 0.6 M$_\odot$ (thick solid line), is suplemented by a CB97 isochrone, available for masses below 0.8 M$_\odot$ (thin line).

References

Abazajian, K.N, Adelman-McCarthy, J.K., Agüeros, M.A. et al. 2009, ApJS, 182, 543
Baraffe, I., Chabrier, G., Allard, F., Hauschildt, P.H. 1998, A&A, 337, 403
Bensby T., Feltzing, S., Lundström, I. 2003, A&A, 410, 527
Bensby, T., Oey M. S., Feltzing S., Gustafsson B., 2007, ApJ, 655, L89
Bessel, M.S., Castelli, F., Plez, B. 1998, A&A, 333, 231
Blake, C.H., Torres, G., Bloom, J.S., Gaudi, B.S. 2008, ApJ, 684, 635
Çakırlı, Ö. & İbanoğlu, C. 2010, MNRAS, 401, 1141
Çakırlı, Ö., İbanoğlu, C. & Güngör, C. 2009, NewA, 14, 496
Caldwell, J.A.R., et al. 1993, SAAO Circulars, 15, 1
Casagrande, L., Portinari, L., Flynn, C. 2006, MNRAS, 373, 13
Castelli, F., Kurucz, R. 2003, IAUS, 210, A20 [arXiv:astro-ph/0405087v1]
Chabrier, G., Baraffe, I. 1997, A&A, 327, 1039
Chabrier, G., Gallardo, J., Baraffe, I. 2007, A&A, 472, L17
Christian, D.J., Mathioudakis, M. 2002, AJ, 123, 2796
Clausen, J.V. 2008, A&A, 487, 1095
Carlsberg Meridian Catalog Number 14, 2006, Copenhagen University Obs., Institute of Astronomy, Cambridge, UK, Real Instituto y Observatorio de la Armada en San Fernando
Coughlin, J.L., Shaw, J.S., JSARA, 1, 7
Cutri, R.M., Skrutskie M.F., Van Dyk S. et al. 2003, *The 2MASS All-Sky Catalog of Point Sources*, University of Massachusetts and Infrared Processing and Analysis Center (IPAC/California Institute of Technology)
Demarque, P., Woo, J.-H., Kim, Y.-C., Yi, S.K. 2004, ApJS, 155, 667
Diaz-Cordovez, J., Gimenez, A. 1992, A&A, 259, 227
Etzel, P.B. 1981, Photometric and Spectroscopic Binary Systems, 111
Fleming, T.A., Gioia, I.M., Maccacaro, T. 1989, ApJ, 340, 1011
Flower, P.J. 1996, ApJ, 469, 355
Girardi, L., Bressan, A., Bertelli, G., Chiosi, C. 2000, A&AS, 141, 371
Girardi, L., Bertelli, G., Bressan, A., Chiosi, C., Groenewegen, M. A. T.; Marigo, P.; Salasnich, B.; Weiss, A. 2002, A&A, 391, 195
Gizis, J.E., Reid, I.N., Hawley, S.L. 2002, AJ, 123, 3356
Harmanec, P.B. 1988, Bull. astr. Inst. Czechosl., 39, 329
Hawley, S.L., Reid, I.N., Tourtellot, J.G., 1999, in ASP Conf. Ser. 158, Solar and Stellar Activity: Similarities and Differences, ed. C.J. Butker & J.G. Doyle, San Francisco: ASP, 63
Hełminiak, K.G., Konacki, M., Ratajczak, M., Muterspaugh, M.W. 2009, MNRAS, 400, 969
Hog E., Fabricius C., Makarov V.V., et al. 2000, A&A, 355, L27
Irwin, J., Aigrain, S., Hodgkin, S., et al. 2007, MNRAS, 380, 541
Irwin, J.,Charbonneau, D., Berta, Z.K., et al. 2009, ApJ, 701, 1436
Jimenez R., Flynn C., Kotoneva E. 1998, MNRAS, 299, 515
Johnson, D.R.H., Soderblom, D.R. 1987, AJ, 93, 864
Kallrath, J., Milone, E.F. 2009, Eclipsing Binary Stars: Modeling and Analysis, 2 ed., Springer, New York
Kałużny, J., Ruciński, S.M., Thompson, I.B., Pych, W., Krzeminski, W. 2007, AJ, 134, 541
Kałużny, J., Thompson, I.B., Ruciński, S.M., Krzemiński, W. 2008, AJ, 136, 400
Kharchenko, N.V. 2001, Kinematika i Fizika Nebesnykh Tel, 17, 409
Konacki, M. 2005, ApJ, 626, 431
Konacki, M., Muterspaugh, M.W., Kulkarni, S.R, Hełminiak, K.G. 2009, ApJ, 704, 513
Konacki, M., Muterspaugh, M.W., Kulkarni, S.R., Hełminiak, K.G. 2010, ApJ, 719, 1293
Kron, G.E. 1952, ApJ, 115, 301
Lacy, C.H. 1977, ApJ, 218, 444
Lacy, C.H.S., Torres, G., Claret, A., Vaz, L.P.R. 2005, AJ, 130, 2838
Lampton, M., Lieu, R., Schmitt, J.H.M.M., Bowyer, S., Voges, W., Lewis, J., Wu, X. 1997, ApJS, 108, 545
Lastennet, E., Valls-Gabaud, D. 2002, A&A, 396, 551
Lejeune, T., Shaerer, D. 2001, A&A, 366, 538
López-Morales, M., Ribas, I. 2005, ApJ, 631, 1120
López-Morales, M. 2007, ApJ, 660, 732
Lucy, L.B. 1967, ZAp, 6, 89
Marigo, P., Girardi, L., Bressan, A., Grönewegen, M.A.T., Silva, L., Granato, G.L. 2008, A&A, 482, 883
Monet, D., Bird A., Canzian B. et al. 1998, The PPM USNO-A2.0 Catalogue
Montes, D., Fernandez-Figueroa, M.J., de Castro, E., Sanz-Forcada, J. 1997, A&AS, 125, 263
Montes, D., Crespo-Chacón, I., Gálvez, M. C., Fernández-Figueroa, M. J. 2007, IAUS, 240, 459
Morales, J.C., et al. 2009a, ApJ, 691, 1400
Morales, J.C., Torres, G., Marschall, L.A., Brehm, W. 2009b, ApJ, 707, 671
Nordström, B., et al. 2004, A&A, 418, 989
Parihan, P., Messina, S., Pama, B., Medhi, B.J., Muneer, S., Velu, C, Ahmad, A. 2009, MNRAS, 395, 593, 607
Pojmański, G. 2002, Acta Astron., 52, 397
Polomski, E., Vennes, S., Thorstensen, J.R., Mathioudakis, M., Falco, E.E. 1997 ApJ, 486, 179
Popper, D.M. 1994, AJ, 108, 1091
Popper, D.M. 1997, AJ, 114, 1195
Popper, D.M., Etzel, P.B. 1981, AJ, 86, 102
Popper, D.M., Lacy, C.H., Frueh, M.L., Turner, A.E. 1986, AJ, 91, 383
Prša, A., Zwitter, T. 2005, ApJ, 628, 426

Prša, A., Zwitter, T. 2006, Ap&SS, 304, 347
Ribas, I. 2003, A&A, 398, 239
Ribas, I., et al. 2008, MmSAI, 79, 562
Röser, S., Schilbach, E., Schwan, H., Kharchenko, N.V., Piskunov, A.E., Scholz, R.-D. 2008, A&A, 488, 401
Różyczka, M., Kałużny, J., Pietrukowicz, P. et al. 2009, Acta Astron., 59, 385
Seabroke, G.M., Gilmore, G. 2007, MNRAS, 380, 1348
Shkolnik, E. et al. 2008, ApJ, 682, 1248
Southworth, J., Maxted, P.F.L., Smalley, B. 2004a, MNRAS, 351, 1277
Southworth, J., Zucker, S., Maxted, P.F.L., Smalley, B. 2004b, MNRAS, 355, 986
Southworth, J., Clausen, J.V. 2007 A&A, 461, 1077
Stassun, K.G., Mathieu, R.D., Cargile, P.A, et al. 2008, Nature, 453, 1079
Stassun, K.G., Mathieu, R.D., Vaz, L.P.R., Stroud, N., Vrba, F.J. 2004, ApJS, 151, 357
Thompson, I.B., Kałużny, J., Pych. W, et al. 2001, AJ, 121, 3089
Thompson, I.B., Kałużny, J., Ruciński, S.M., et al. 2010, AJ, 139, 329
Tokunaga, A.T. 2000 in Allens' Astrophysical Quantities, 4th edition, ed. A.N. Cox, Springer-Verlag, p.143
Torres, G., Ribas, I. 2002, ApJ, 567, 1140
Torres, G., Andersen, J., Gimenéz, A. 2010 A&A Rev., 18, 67
Urban, S.E., Corbin, T.E., Wycoff, G.L., Makarov, V.V., Hog, E., Fabricius, C. 2001, BAAS, 33, 1494
Vaccaro, T.R. et al. 2007, ApJ, 661, 1112
van Hamme, W. 1993, AJ, 106, 2096
van Leeuwen, F. 2007, A&A, 474, 653
Voges, W. et al. 1999, A&A, 349, 389
Wilson, R.E., Devinney, E.J. 1971, ApJ, 166, 605
Yi, S. et al 2001, ApJS, 136, 417
Zhao, J., Zhao, G., Chen, Y. 2009, ApJ, 692, L113
Zucker, S., Mazeh, T. 1994, ApJ, 420, 806